J. Bangladesh Acad. Sci. 46(2); 193-202: December 2022 DOI:10.3329/jbas.v46i2.63046

Journal of Bangladesh Academy of Sciences

Journal homepage: http://www.bas.org.bd/publications/jbas.html

Research Article

Total variation denoising and Euclidean distance based distributed temperature monitoring in Brillouin optical time-domain analysis sensors

Taskin Sakin, Tanbin Ahmed and Abul Kalam Azad*

Department of Electrical and Electronic Engineering, University of Dhaka, Bangladesh

ARTICLE INFO

Article History

Received:1 December 2022
Revised: 18 December 2022
Accepted: 20 December 2022

Keywords: Distributed fiber optic sensors, Total variation denoising, Euclidean distance, Least-squares fitting, Pattern recognition.

ABSTRACT

The performance of Brillouin optical time domain analysis (BOTDA) sensors is largely deteriorated due to the poor signal-to-noise ratio (SNR) of Brillouin gain spectra (BGSs) collected from the BOTDA experiment. The fast monitoring of distributed temperature using BOTDA sensors is also vital for many long-distant applications. To cope with these requirements, this paper proposes total variation denoising (TVD) and Euclidean distance-based pattern recognition (TEPR) for high-performance BOTDA sensors. The performances of TEPR are analyzed explicitly, and rigorous comparisons have been made with traditional nonlinear least squares fitting (NLSF). The experimentally demonstrated results signify that the proposed TEPR can improve the measurement uncertainty by up to ~55% compared to NLSF without worsening the experimental spatial resolution. The signal processing for using TEPR is also ~4 times faster than that for using NLSF. Hence, the proposed technique is an efficient and reliable alternative for the fast and accurate monitoring of distributed temperature in BOTDA sensors.

Introduction

In recent decades, stimulated Brillouin scattering (SBS) based BOTDA sensors have exhibited enormous capabilities in the distributed monitoring of temperature and strain (Motil et al, 2016; Azad et al., 2017; Ba et al., 2016). Such sensors offer high accuracy, good spatial resolution and long-distant monitoring even in hazardous environments (Azad et al., 2017; Wang et al., 2020). For the distributed monitoring of temperature, BOTDA sensors exploit an amplified probe wave which becomes amplified as a result of interaction with the oppositely-directed pump wave through a single piece of optical fiber cable (OFC). The gain in this amplification process is recorded as local Brillouin gain spectrum (BGS) along the OFC. The difference in pump-probe frequency (f_d) for which peak gain is attained in a local BGS is termed in literature as the local Brillouin frequency shift (BFS) (Motil et al, 2016; Zhao et al., 2022). The BFS of a local BGS alters linearly with the surrounding temperature of OFC. In the BOTDA experiment, the local BGSs along the OFC are assembled with BOTDA traces collected by varying f_d step-by-step within a suitable frequency range. In temperature monitoring applications, BFSs of the local BGSs are first determined, which are then mapped to temperature according to the linear BFS-temperature relationship (Azad et al., 2017). To determine such BFSs, NLSF is a widely-used technique (Azad et al., 2017; Haneef et al., 2018).

A single BOTDA trace collected from the conventional BOTDA sensor at a particular f_d is very noisy. The SNR of BGSs formed with such noisy traces is thus very low. The performance of

*Corresponding author: <azad@du.ac.bd>

BOTDA sensors also deteriorates for such low SNR. The SNR of BGSs along OFC can effectively be improved to an acceptable level by adopting a trace-averaging approach. Such an approach requires the gathering a large number of traces (e.g., several thousand) at a particular f_d, which are then averaged to attain one averaged trace at that f_d to be used for constructing BGSs. This averaging approach is time-intensive and thus lengthens the collection of BGSs, especially for long OFC if the number of traces (T_N) averaged is quite large.

For the fast collection of BGSs with improved SNR, several alternative schemes have been combined with conventional BOTDA sensors. The studies (Jia et al., 2010; Angulo-Vinuesa et al., 2012) combined Raman amplification with BOTDA sensors to enhance the sensing performance. Alternatively, the realizations of long-distant sensing using pulse coding techniques have been reported in Ref. (Iribas et al., 2017; Mariñelarena et al., 2018). The combination of Raman amplification and pulse coding technique has also been reported to attain high-performance sensing with improved accuracy and resolution (Soto et al., 2012). However, the combination of such additional schemes to conventional BOTDA sensors makes the BOTDA setup complex and costly due to the use of additional hardware components.

Other than employing the complex, costly and modified BOTDA setup, a viable alternative is to collect much noisy BGSs along the OFC, adopting a small number of trace averaging (i.e., smaller T_N) with conventional BOTDA setup and then using an effective and time-efficient denoising algorithm for denoising such noisy BGSs. To explore this, several signal denoising techniques, such as wavelet transform (Soto et al., 2016; Azad, 2020), Wiener filter (Azad, 2022), non-local means filter (Qian et al., 2017; Soto et al., 2017) and anisotropic diffusion filter (Luo et al., 2020; Zhang et al., 2022) have been proposed and demonstrated to enhance the SNR of the BGSs along the OFC. The study Liu et al.(2022) shows significant improvement in measurement uncertainty by using one-dimensional denoising convolutional neural network (1D-DnCNN) for a 6 km OFC in Raman scattering-based distributed optical fiber sensor. In addition, the use of general regression neural network (GRNN) has proven superior for accurate temperature extraction in BOTDA sensors (Zhou et al., 2021). A comprehensive review of recent research works presented in (Venketeswaran et al., 2021) also reports the advantages of using signal-denoising algorithms to enhance measurement accuracy of fiber optic sensors. However, such a denoising technique includes extra runtime in processing BGSs. Moreover, the determination of BFSs from local BGSs is usually performed by applying NLSF. The operating principle of NLSF is based on the process of iterative optimization, which entails substantial time to determine BFSs if a great number of BGSs is required to be processed for the distributed monitoring of temperature throughout a long OFC. Consequently, high-speed signal processing techniques are essential for fast monitoring of distributed temperature in BOTDA sensors.

Within this framework, we have proposed using total variation denoising (TVD) to improve the SNR of BGSs collected from BOTDA experiment. The SNR improvements due to the use of TVD have been analyzed explicitly for the BGSs collected with ten different T_N. We have also proposed TVD and Euclidean distance-based pattern recognition (TEPR) for distributed temperature monitoring over 38.2 km OFC. The performances of TEPR have been evaluated rigorously in terms of measurement uncertainty, spatial resolution and signal processing speed.

Experimental Setup

The collection of BGSs along the OFC has been accomplished via the conventional BOTDA setup (Azad et al., 2017) shown in Fig. 1.

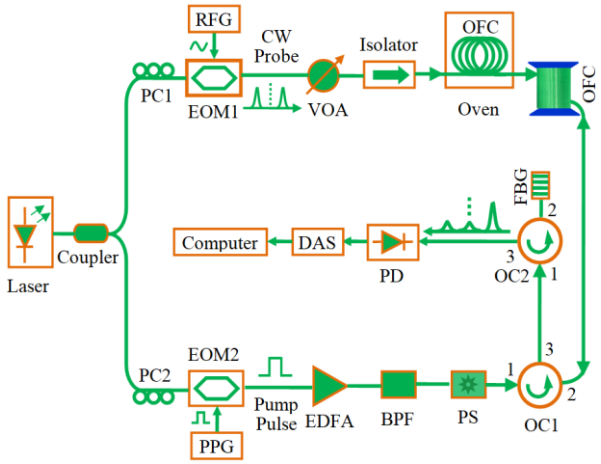

Fig. 1. Setup of BOTDA sensor

As shown in Fig. 1, the beam of light outputted by a CW-laser at 1550 nm is divided by the coupler to launch through the setup. The split beams pass through polarization controllers PC1 and PC2 to control the polarization state of light beams. To form double-sideband suppressed-carrier probe signal in the upper branch, the output of a radio frequency generator (RFG) is inputted to the electro-optic modulator (EOM1). The power of the probe light is tuned with the variable optical attenuator (VOA). Afterward, the isolator restricts the propagation of pump pulses from the reverse path but assists the probe signal to be passed through it in the forward direction to the far end of the OFC.

To generate pump pulses in the lower branch, the second electro-optic modulator (EOM2) is used. This EOM2 is assisted by the pulse-pattern generator (PPG). The pump pulses are next amplified by the erbium-doped fiber amplifier (EDFA). In this amplification process, the spontaneous emission noise also becomes amplified, which is eliminated by the band-pass filter (BPF). The polarization scrambler (PS) in the lower branch helps to diminish fading of Brillouin gain. These pump pulses are then directed from port 1 to port 2 of the optical circulator (OC1) to be launched through the near end of the OFC.

Two oppositely directed signals (i.e., pump and probe) interact inside the OFC via SBS, and both the lower and upper sidebands of the probe signal get amplified. The upper sideband is next nullified by the fiber Bragg grating (FBG) filter connected at port 2 of optical the circulator (OC2) and the photodetector then detects the desired lower sideband. The data acquisition system (DAS) acquires BOTDA traces. These traces are stored in the computer and used to form local BGSs along the OFC. These BGSs are finally processed to monitor the distributed temperature along the OFC.

Operating Principle

In our work, the experimental noisy BGSs collected throughout the OFC have been denoised first by utilizing total variation denoising (TVD). Then, a database comprising relevant ideal BGSs was constructed. Finally, Euclidean distance based pattern recognition has been applied among the denoised BGSs along the OFC and the ideal BGSs in the database to determine the temperature distribution from the experimental BGSs.

Total variation denoising (TVD) is a widely-used technique for reducing the total variation of an image and eliminating undesirable information while maintaining important details, such as edges (Rudin et al., 1992; Tang and Fang, 2016; Kamalaveni et al., 2018; Jin and Luan, 2020). This study considers the combined noisy BGSs along the OFC as a 2D image *B*. Such noisy image comprising experimental BGSs can be modeled as follows:

$$B(p,q) = D(p,q) + n(p,q) \quad (1)$$

Where $D(p,q)$ is the original image corrupted by the noise $n(p,q)$ and (p,q) is the pixel position in image $B(p,q)$. Due to the random nature of $n(p,q)$, the total variation (TV) in $D(p,q)$ is much smaller than that in $B(p,q)$. Consequently, the denoising of $B(p,q)$ is to find an estimate of $D(p,q)$ having smaller TV than that of $B(p,q)$ (Rudin et al., 1992). In such a process of TVD, the estimated image should also be well-matched with $B(p,q)$. This can be accomplished using TVD by minimizing the energy function given by (Liao et al., 2015; Kamalaveni et al., 2018)

$$\min_{B} E(D) = \int_{\Omega} |\nabla D| dpdq + \lambda \int_{\Omega} (D - B)^2 dpdq \qquad (2)$$

where Ω is the total number of pixels in $B(p,q)$, $|\nabla D(p,q)|$ is the gradient magnitude at position (p,q), and λ is the regularization parameter (Kamalaveni et al., 2018). The proper choice of λ controls the balance between the denoising level of $B(p,q)$ and the matching of the denoised image with $D(p,q)$ (Liao et al., 2015).

The denoised image D obtained after applying TVD consists of a denoised version of experimental noisy BGSs in B. The denoised BGSs in D are next processed using Euclidean distance-based pattern recognition to monitor the distributed temperature along the OFC. Such process (i.e., TEPR) is depicted in Fig. 2.

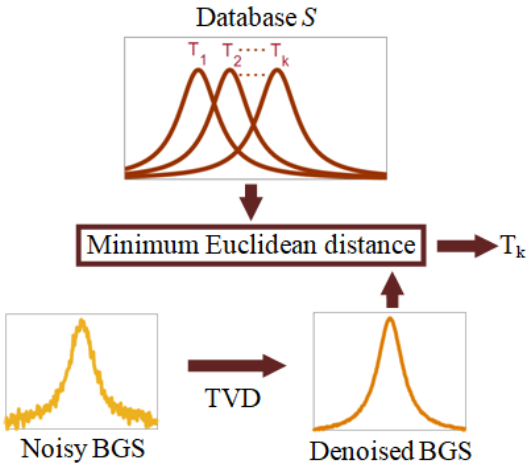

Fig. 2. The process of temperature monitoring using TEPR

As illustrated in Fig. 2, the temperature monitoring using the proposed technique of TEPR uses a database S comprising numerous ideal BGSs associated with known temperature. The process of constructing such a database will be analyzed in detail later in the results and discussion section. To apply TEPR, the experimental noisy BGSs along the OFC are first denoised by TVD. The denoised BGSs in D are then matched with the ideal BGSs in S, as shown in Fig. 2. For each BGS in D, we determine its best match with the ideal BGSs in S. This best match is defined in terms of minimum Euclidean distance. If the BGSs in S and D are represented by vectors s and d, respectively each having m data points, the Euclidean distance (l) between s and d is then given by (Azad et al., 2017)

$$l(s,d) = \sqrt{\sum_{i=1}^{m} (s_i - d_i)^2} \qquad (3)$$

The known temperature associated with the best-matched ideal BGS in S is designated as the temperature associated with the experimental noisy BGS. The process is repeated for all the experimental BGSs along the OFC for the distributed temperature monitoring throughout the 38.2 km OFC.

To compare the performance of TEPR, we also determine the temperature distributions directly from the experimentally noisy BGSs by applying NLSF. Since the BOTDA-measured BGSs are ideally modeled by the Lorentzian function (Azad et al., 2017; Haneef et al., 2018), we have utilized this function in NLSF. Such function is given by

$$g(\upsilon) = \frac{g_B}{1 + 4\left[(\upsilon - \upsilon_B)/(\Delta\upsilon_B)\right]^2} \qquad (4)$$

where g_B, υ_B and $\Delta\upsilon_B$ are termed as the peak gain, BFS and linewidth of the BGS, respectively. In NLSF, the parameters g_B, υ_B and $\Delta\upsilon_B$ of function given by Eq. (4) are updated iteratively to find the best-fit between this function and the BGS in term of least-squares error. The updated υ_B is estimated to be the BFS of the BGS used in NLSF. It is worth to mention that the SNR of experimental noisy BGS as well that of denoised BGS obtained after applying TVD has been calculated (Azad et al., 2017) in this study by

$$\mathrm{SNR(dB)} = 10\log_{10}\left(\frac{g_B^2}{\sigma^2}\right) \qquad (5)$$

where σ^2 is the variance of residuals (i.e., differences between the fitted and observed BGSs) in NLSF.

Results and Discussion

In our experiment, we used a 38.2 km long OFC in the BOTDA sensor shown in Fig. 1. We put ~600 m

fiber from the last part of the OFC into an oven and the temperature of the oven was set at 70°C. To collect local BGSs at every 0.4 m along the OFC, BOTDA-traces have been collected at a sampling rate of 250 MHz. The BGSs have been collected for the frequency range from 10.76 GHz to 11.01 GHz with 1 MHz spacing. The width of pump pulses has been fixed to 20 ns to realize a 2 m spatial resolution. The BGSs along the OFC have been collected by adopting ten T_N (i.e., T_N =100 to 1000 with a step of 100). The experimental BGSs along the OFC obtained for T_N = 100 and their corresponding denoised BGSs obtained after applying TVD are shown in Fig. 3 (a) and (b), respectively.

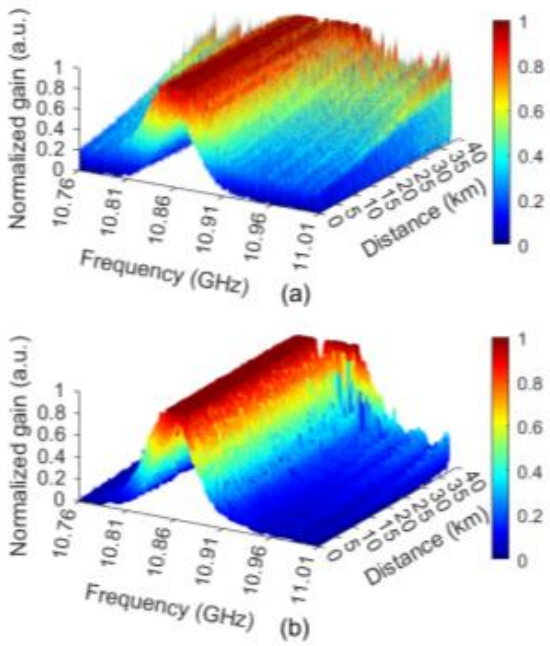

Fig. 3. Distributions of (a) experimental noisy BGSs and (b) denoised BGSs

It is observed that the level of noise in BGSs shown in Fig. 3(a) is much higher, which has been improved radically due to the use of TVD, as shown in Fig. 3(b). To observe the SNRs of noisy and denoised BGSs, we have next computed the SNRs of BGSs along the OFC shown in Fig. 3 by applying Eq. (5). Such SNRs for T_N = 100 are shown in Fig. 4.

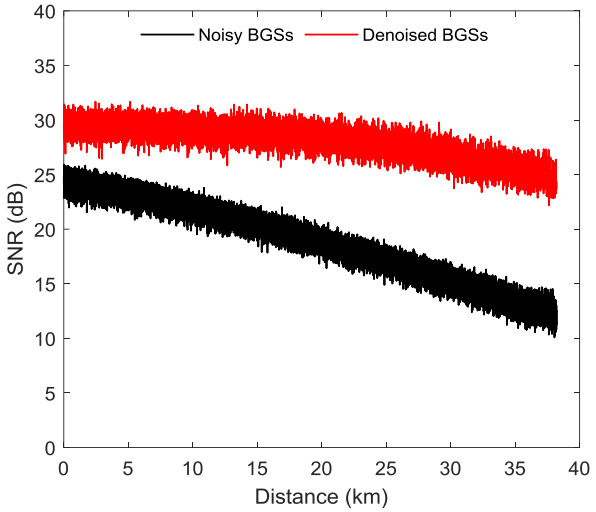

Fig. 4. SNRs of BGSs along the optical fiber

The results in Fig. 4 indicate that the SNRs of experimental noisy BGSs vary along the 38.2 km OFC, notably mainly due to fiber attenuation (Azad, 2022). However, the use of TVD on the noisy BGSs manifests a significant improvement in SNR, especially at the end of OFC, where the SNRs of noisy BGSs are the lowest. To quantify the variation of SNRs with T_N, we have also computed the average SNR of the BGSs along the last 500 m OFC. The results are shown in Fig. 5.

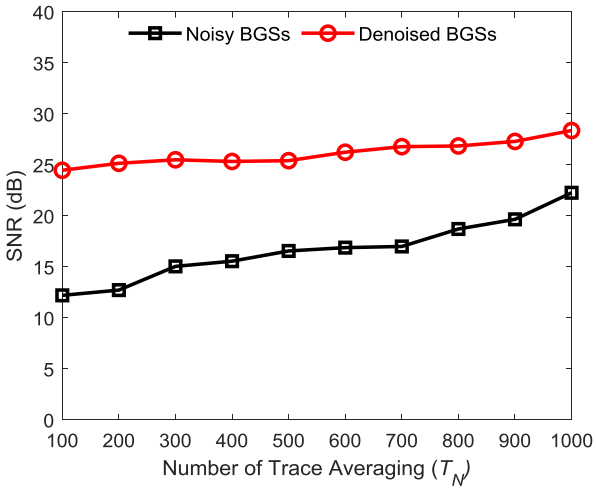

Fig. 5. Average SNR of BGSs along the last 500 m optical fiber

It can be observed in Fig. 5 that the SNRs of experimental BGSs increase if a larger T_N is

adopted to collect BGSs. For instance, the average SNR of experimental noisy BGSs in Fig. 5 varies from its lowest value of 12.21 dB to its highest value of 22.27 dB for adopting T_N = 100 and T_N = 1000, respectively. However, TVD-based NLSF can provide many improved SNRs of 24.48 dB and 28.37 dB for the same T_N of 100 and 1000, respectively. Consequently, TVD can improve the SNR by 12.27 dB and 6.10 dB for the BGSs collected with T_N of 100 and 1000, respectively. Notably, the improvement of SNR at smaller T_N in Fig. 5 is much larger than that at larger T_N. This is because the average SNR of BGSs at higher T_N is already much better as compared to that at lower T_N. For the BGSs having such higher SNR, TVD has a little to improve. The results in Fig. 5 signify that TVD can offer significantly improved SNR, which also helps to improve the measurement uncertainty of the BOTDA sensors.

As mentioned earlier, the operating principle of TEPR is based on the database comprising ideal BGSs. The BGSs in such a database should ideally mimic the BGSs obtained from the BOTDA experiment under various experimental conditions (e.g., fiber length, temperature, and pump-pulse width). In this study, the ideal BGSs in the database are constructed with the Lorentzian function given by Eq. (4). For using Eq. (4), the peak gain of the ideal BGSs is normalized to be g_B = 1. To monitor temperature within the range from 0 ºC to 100 ºC using the BOTDA sensor, υ_B (BFS) of each BGS in the database has been varied within the range from 10.834 GHz to 10.932 GHz (with the BFS spacing of 0.2 MHz) depending on the characteristics (i.e., intercept of ~10.83415 GHz and slope of ~0.97497 MHz/ºC) of the OFC (Azad et al., 2017; Azad, 2022). The linewidth ($\Delta\upsilon_B$) to be used in Eq. (4) has been decided based on the linewidths of the experimental BGSs. To decide so, we have first denoised the experimental noisy BGSs by applying TVD. The linewidths of the denoised BGSs are then determined by utilizing NLSF. For adopting 20 ns pump-pulse during the BOTDA experiment, the linewidths of such denoised BGSs for T_N =1000 (the highest T_N used in this study) are shown in Fig. 6. The average linewidth within every 1 km OFC are also plotted in Fig. 6.

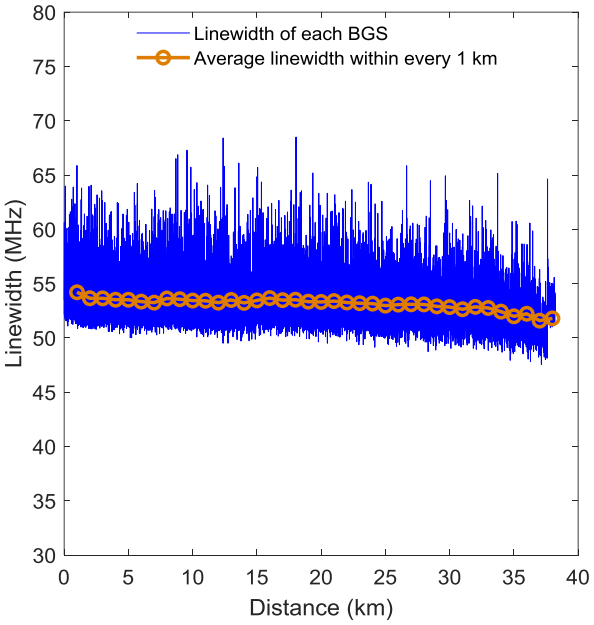

Fig. 6. Variation of the linewidth of BGSs along the optical fiber

It is noticed in Fig. 6 that the average linewidths within every 1 km OFC are ~53 MHz. Consequently, we have set $\Delta\upsilon_B$ = 53 MHz in Eq. (4) for constructing the database. For monitoring temperatures from 0 ºC to 100 ºC, the database thus contains a total of k = 491 ideal BGSs.

Next, we have evaluated the suitability of using TEPR and the constructed database for monitoring temperature distributions from the local BGSs along the OFC collected by adopting different T_N. The process of such a monitoring system is depicted in Fig. 2, in which the experimental noisy BGSs along the OFC are first denoised by applying TVD. Then, we have found the best match between each denoised BGS along the OFC and ideal BGSs in the database based on minimum Euclidean distance. The temperature distribution provided by TEPR for local BGSs collected at T_N = 100 is shown in Fig. 7. The

temperature distribution obtained for applying NLSF on experimental noisy BGSs at T_N = 100 are also shown in Fig. 7 for comparison.

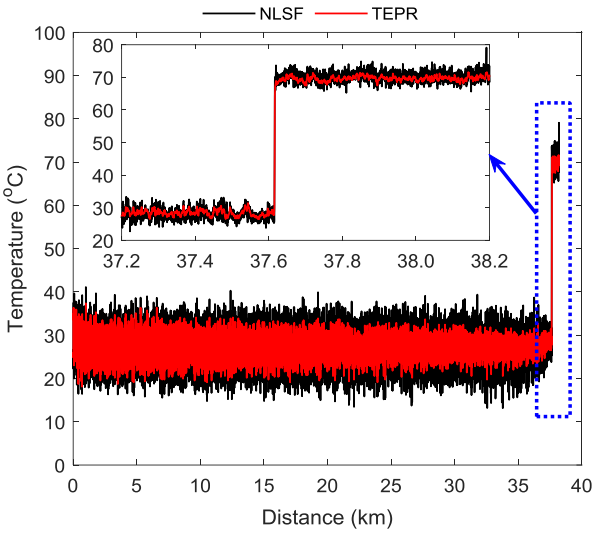

Fig. 7. Temperature distributions along the optical fiber

It is clear from Fig. 7 that the temperature fluctuations provided by TEPR are much smaller than that provided by NLSF. The smaller fluctuations in the temperature distribution due to the use of TEPR offer much reduced uncertainties in monitoring distributed temperature.

The denoising algorithm operation relies on eliminating the signals' high-frequency components (Azad, 2022). For such algorithm in BOTDA sensors, the BGSs along the OFC can be over-smoothed which can also deteriorate the experimental spatial resolution. To examine this, the distributions of temperature provided by NLSF and TEPR are plotted in Fig. 8 along the section of the OFC at which the distributions rise sharply from room temperature to 70 ºC. Such temperature distributions confirm that TEPR can maintain the experimental spatial resolution, which is 2 m in our study for adopting 20 ns pump-pulse.

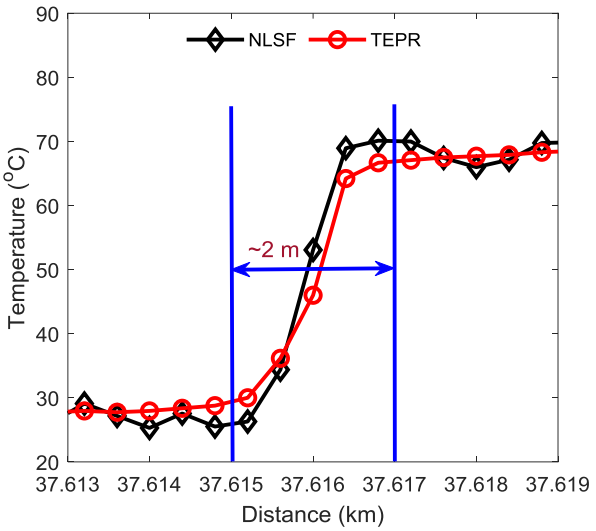

Fig. 8. Spatial resolution of the sensor

The results presented in Figs. 4 and 5 specify that the use of TVD can notably improve the SNR of the experimental BGSs. As a result, the fluctuations in the temperature distributions also reduce significantly as can be seen in Fig. 7. To quantify the reduction of such fluctuations, we have computed the uncertainties in monitoring temperature distributions. The uncertainty for each T_N is defined as the standard deviation of temperatures along the last 500 m OFC heated inside the oven. The results are plotted in Fig. 9.

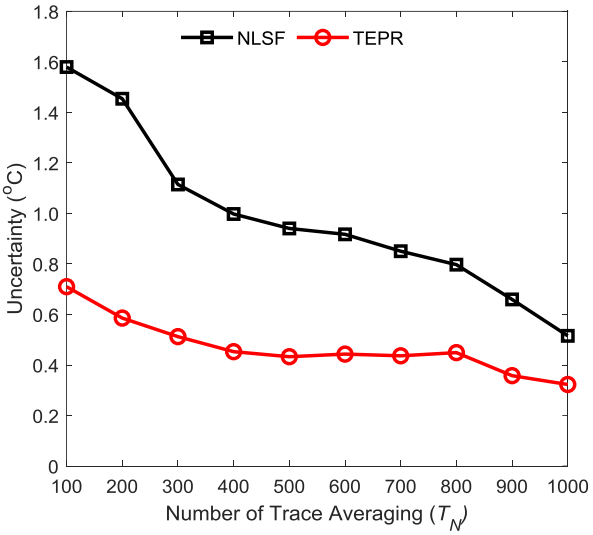

Fig. 9. Uncertainty in temperature monitoring

The results in Fig. 9 confirm that using TEPR provides significantly reduced measurement uncertainties compared to NLSF for each T_N adopted in this study. For instance, the uncertainty provided by NLSF for T_N = 100 is 1.58 ºC for the BGSs along the last 500 m fiber having SNR of 12.21 dB as shown in Fig. 5. For the same T_N, TEPR can provide much-reduced uncertainty of 0.71 ºC. Consequently, using TEPR can improve the measurement uncertainty by 55.06% at T_N = 100, the lowest T_N (i.e., lowest SNR of 12.21 dB) adopted in this study. This improvement in measurement uncertainty is much better than ~44.60% as reported by Zhoua et al.(2021), in which the use of GRNN and curve fitting method (i.e., NLSF) can provide root-mean-square errors of ~0.36 ºC and ~0.65 ºC, respectively, for the BGSs having similar SNR of 12 dB. However, the improvement of uncertainties for adopting higher T_N, such as T_N of 400, 700, and 1000 are 54.61%, 48.68% and 37.36%, respectively. These results suggest that the improvement of uncertainties decreases if a larger T_N is adopted to collect the BGSs from the BOTDA experiment. This is because the SNRs of the local BGSs collected at larger T_N is also larger. In such cases, the denoising of BGSs using TVD can improve the SNRs a little, as the noise level in the experimental BGSs is already much smaller.

Finally, we have compared the speed of NLSF and TEPR in monitoring the temperature distributions along the OFC. To do so, we have computed the runtimes taken by NLSF and TEPR to monitor temperature distributions from the local BGSs collected at different T_N. In the calculation of runtimes of TEPR, we have included the runtime taken by TVD and that taken by Euclidean distance-based pattern recognition. The speed of TEPR is calculated in terms of relative runtimes, which are the ratios of runtimes taken by NLSF to that taken by TEPR for each T_N. The results are shown in Fig. 10.

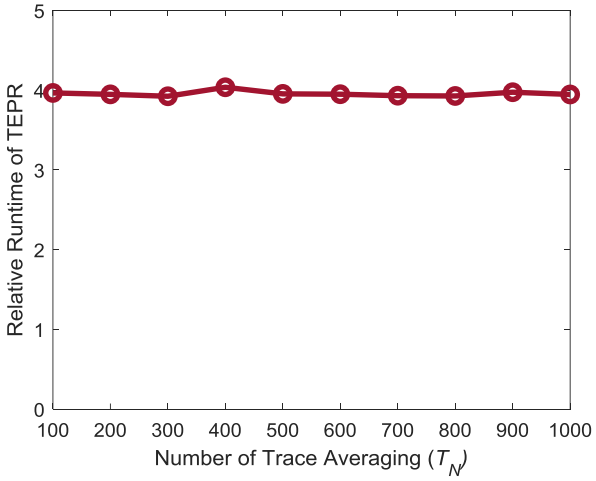

Fig. 10. Relative runtime of TEPR

It is clear from Fig. 10 that the relative runtimes of TEPR for different T_N are almost the same. The results in Fig. 10 signify that the monitoring of distributed temperature using TEPR is ~4 times faster than that of NLSF. It is worth mentioning that the use of GRNN (Zhou et al., 2021) can provide ~7 times faster processing speed over NLSF but can offer a 44.60% improvement of measurement uncertainty which is much lower than that of 55.06% achieved in this study.

Conclusion

This paper represents a rigorous study using TVD and Euclidean distance-based pattern recognition (TEPR) for the distributed temperature monitoring in BOTDA sensors. The TVD is first used to denoise the experimental BGSs. Then, a custom-made database comprising ideal BGSs is constructed and used by the Euclidean distance-based pattern recognition technique to monitor the distributed temperature along a 38.2 km optical fiber cable. The results show that the use of TVD can significantly improve the SNR of experimental BGSs up to 12.27 dB. Consequently, TEPR can improve the measurement uncertainty by up to 55.06% compared to NLSF without worsening the spatial resolution of BOTDA sensors. In addition, the signal processing speed of the proposed TEPR is ~4 times faster than that of NLSF. Therefore, the proposed TEPR can serve as a potential tool for

high-performance monitoring of distributed temperature using BOTDA sensors.

Acknowledgments

The authors are grateful to the University of Dhaka, Bangladesh, for the financial support of this work under the Centennial Research Grant (CRG). The authors also acknowledge the support of the 'Photonics Research Institute' at The Hong Kong Polytechnic University, Hong Kong SAR, for the facility of the experiment.

References

Angulo-Vinuesa X, Martin-Lopez S, Corredera P and Gonz´alez-Herr´aez M. Raman-assisted Brillouin optical timedomain analysis with sub-meter resolution over 100 km. Opt. Exp. 2012; 20(11): 12147-12154.

Azad AK, Khan FN, Alarashi WH, Guo N, Lau APT and Lu C. Temperature extraction in Brillouin optical time-domain analysis sensors using principal component analysis based pattern recognition. Opt. Exp. 2017; 25(14):16534-16549.

Azad AK. Analysis of 2D Discretewavelet transform based signal denoising technique in brillouin optical time domain analysis sensors. Dhaka Univ. J. App. Sci. Engg. 2020; 5(1&2):1-8.

Azad AK. Extraction of temperature distributions in brillouin optical time domain analysis sensors using 2D wiener filter based matched filter detection. Dhaka Univ. J. App. Sci. & Engg. 2022; 6(2): 30-38.

Ba D, Wang B, Zhou D, Yin M, Dong Y, Li H, Lu Z and Fan Z.Distributed measurement of dynamic strain based on multislope assisted fast BOTDA. Opt. Exp. 2016; 24(9): 9781-9793.

Haneef SM, Yang Z, Thévenaz L, Venkitesh D and Srinivasan B. Performance analysis of frequency shift estimation techniques in Brillouin distributed fiber sensors. Opt. Exp. 2018; 26(11): 14661-14677.

Iribas H, Loayssa A, Sauser F, Llera M and Floch SL. Cyclic coding for Brillouinoptical time-domain analyzer using probe dithering. Opt. Exp. 2017; 25(8): 8787-8800.

Jia X, Rao Y, Chang L, Zhang C and Ran Z. Enhanced sensing performance in long distance Brillouin optical time-domain analyzer based on Raman amplification: Theoretical and experimental investigation. J. Lightwave Technol. 2010; 28(11): 1624–1630.

Jin C and Luan N. An image denoising iterative approach based on total variation and weighting function. Multimed Tools App.2020; 79: 20947–20971.

Kamalaveni V, Narayanankutty KA, Veni S and Soman KP. Survey on Total Variation based Image Regularization Algorithms for Image Denoising. Int. J. Pure App. Math. 2018; 118(20): 3723-3730.

Liao CH, Choi JH,Zhang D,Chan SH and Cheng JX. Denoisingstimulated Raman spectroscopic images by total variation minimization. J. Physical Chem. 2015; 119(33): 19397-19403.

Liu Z, Wu H, Du H, Luo Z and Tang M. Distributed temperature and curvature sensing based on Raman scattering in Few-Mode fiber. IEEE Sensors J. 2022; 22(23): 22620-22626.

Luo K, Wang B, Guo N, Yu K, Changyuan Yu C and Lu C. Enhancing SNR by anisotropic diffusion for brillouin distributed optical fiber sensors. J. Lightwave Technol. 2020; 38(20): 5844-5852.

Mariñelarena J, Iribas H and Loayssa A. Pulse coding linearization for Brillouin optical time-domain analysis sensors. Opt. Lett. 2018; 43(22):5607-5610.

Motil A, Bergman A and Tur M. State of the art of Brillouin fiber-optic distributed sensing. Opt. Laser Technol. 2016; 78: 81-103.

Qian X, Jia X, Wang Z, Zhang B, Xue N, Sun W, He Q and Wu H. Noise level estimation of BOTDA for optimal non-local means denoising. Appl. Opt. 2017; 56(16): 4727-4734.

Rudin LI, Osher S and Fatemi E. Nonlinear total variation based noise removal algorithms. Physica D: Nonlinear Phenom. 1992; 60(1-4): 259-268.

Soto MA, Ramírez JA and Thévenaz L. Intensifying the response of distributed optical fibre sensors using 2D and 3D image restoration. Nat. Com. 2016; 7: 10870.

Soto MA, Ramírez JA and Thévenaz L. Optimizing image denoising for long-range Brillouindistributed fiber sensing. J. Lightwave Techno. 2017; 36(4): 1168-1177.

Soto MA, Taki M, Bolognini G and Pasquale FD. Simplex-coded BOTDA sensors over 120 km SMF with 1-m spatial resolution assisted by optimized bidirectional Raman amplification. IEEE Photon. Tech. Lett. 2012; 24(20): 1823-1826.

Tang L and Fang Z. Edge and contrast preserving in total variation image denoising. EURASIP J. Adv. Signal Process. 2016; 13: 1-21.

Venketeswaran A, Lalam N,Wuenschell J,Ohodnicki PR, Badar M, Chen KP, Lu P, Duan Y, Chorpening B and Buric M. Recent advances in machine learning for fiber optic sensor applications. Adv, Intell. Syst. 2021; 4: 2100067.

Wang S, Yang Z, Zaslawski S and Thévenaz L. Short spatial resolution retrieval from a long pulse Brillouin optical time-domain analysis trace. Opt. Lett.2020; 45(15): 4152-4155.

Zhang P, Wang B, Yang Y, Azad AK, Luo K, Yu K, Yu C and Lu C. SNR enhancement for Brillouin distributed optical fiber sensors based on asynchronous control. Opt. Exp. 2022; 30(3): 4231-4248.

Zhao L, Chen Y, Xu Z, Zhang X and Mou Q. Brillouin frequency shift error estimation formula for distributed optical fiber sensing technology based on Brillouin scattering. Appl. Opt. 2022; 61: 4354-4362.

Zhou H, Zhu H, Zhang Y, Huang M and Li G. Fast and accurate temperature extraction via general regression neural network for BOTDA sensors. In: Proceedings of SPIE, Vol. 12057. Ed. Yang Y.Twelfth International Conference on Information Optics and Photonics, 120573O-1;2021